

*Letter to the Editor***A Vega-like disk associated with the planetary system of ρ^1 Cnc *****C. Dominik¹, R.J. Laureijs², M. Jourdain de Muizon^{3,4}, and H.J. Habing¹**¹ Sterrewacht, Leiden, P.O. Box 9513, 2300 RA Leiden, The Netherlands² ISO Science Operations Center, Astrophysics Division of ESA, Vilspa, P.O. Box 50727, E-28080 Madrid, Spain³ DESPA, Observatoire de Paris, F-92190 Meudon, France⁴ LAEFF-INTA, ESA Vilspa, P.O. Box 50727, E-28080 Madrid, Spain

Received 2 October 1997 / Accepted 24 October 1997

Abstract. The star ρ^1 Cnc is among the first 10 stars which have been shown to host a planet. Following the discovery of the planet in 1996 we have obtained ISO observations in May 1996. The observations show that ρ^1 Cnc has a $25\ \mu\text{m}$ flux consistent (within the errors) with photospheric origin, and an excess of 170 ± 30 mJy at $60\ \mu\text{m}$. We interpret this excess as emission from dust grains in a Vega-like disk located approximately 60 AU from the star, containing at least $4 \times 10^{-5} M_{\oplus}$ of material.

Key words: stars: planetary systems – stars: general – stars: individual: ρ^1 Cnc – Infrared: stars

1. Introduction

The last two years have witnessed the first detections of extra-solar planets. Following the discovery of a planet near 51 Peg by Mayor & Queloz (1995) and similar results for 47 UMa, 70 Vir and HD 114762, the discovery of 3 new cases was announced by Butler et al. (1997). Among these stars is ρ^1 Cnc (HR 3522, HD 75732). ρ^1 Cnc is a solar-type star with spectral class G8V, slightly metal-rich, at a distance of 12.5 pc. Its age inferred from CaII H and K fluxes is 5 Gyr Baliunas et al. 1997. According to Butler et al. (1997), the planet near ρ^1 Cnc has a period of 14.65 days implying a semi major axis of 0.11 AU. The inferred mass is $M_2 \sin i = 0.84 M_{\text{Jup}}$. This is one of the 51 Pegasi-like “hot Jupiter” planets. The Doppler velocity of the primary also exhibits a long term trend consistent with a second, as yet unconfirmed companion ($P > 8\text{yr}$, $M_3 \sin i > 5 M_{\text{Jup}}$). ρ^1 Cnc is also a resolved double star with an M5 dwarf companion (HD

75732B, $V = 13.15$) at a distance of approximately 1150 AU from the primary.

In 1983 IRAS detected infrared excess from several main-sequence stars, e.g. Vega, β Pic, Formalhaut. This excess was attributed to a disk of dust around the star, which was later confirmed dramatically in the case of β Pic by the observation of scattered light from the disk. Subsequent analysis of the IRAS data base showed that this phenomenon was widely spread among main-sequence stars Aumann et al. 1984, Aumann 1985. The detection of planets around other main sequence stars raised the question whether planets and Vega-like disks can exist together. Unfortunately, the star ρ^1 Cnc was not on any target list for ISO. We therefore applied for discretionary time which was subsequently granted. ISOPHOT measurements were obtained only a few days before the star disappeared from ISO’s visibility zone.

2. Observations

We obtained data with the ISOPHOT instrument (Lemke et al., 1996) on board of the ISO satellite (Kessler et al. 1996) and used AOT (Astronomical Observation Template) PHT03 at $25\ \mu\text{m}$ and PHT22 at 60, 90, 135, and $180\ \mu\text{m}$. ρ^1 Cnc is 4.7 arcmin away from the MIII star HD 75716 which is a relatively bright IRAS source (IRAS 08494+2826) with fluxes of 13.4 and 3.5 Jy at 12 and $25\ \mu\text{m}$ respectively. Calibration observations performed at a later stage on brighter targets have shown that straylight from HD 75716 as an infrared source is negligible. However, detection of this star by ISOPHOT would cause a significant detector responsivity drift which could hinder accurate measurement of the weaker fluxes of ρ^1 Cnc. We therefore designed a 3 points raster scan observation with scan direction approximately perpendicular to the vector defined by HD 75716 and ρ^1 Cnc (scan position angle is 135 degrees). The second raster pointing is centered on ρ^1 Cnc, the first and third pointings measure the background level. For each filter measurement,

Send offprint requests to: C. Dominik

* Based on observations with ISO, an ESA project with instruments funded by ESA Member States (especially the PI countries: France, Germany, The Netherlands and the United Kingdom) and with the participation of ISAS and NASA.

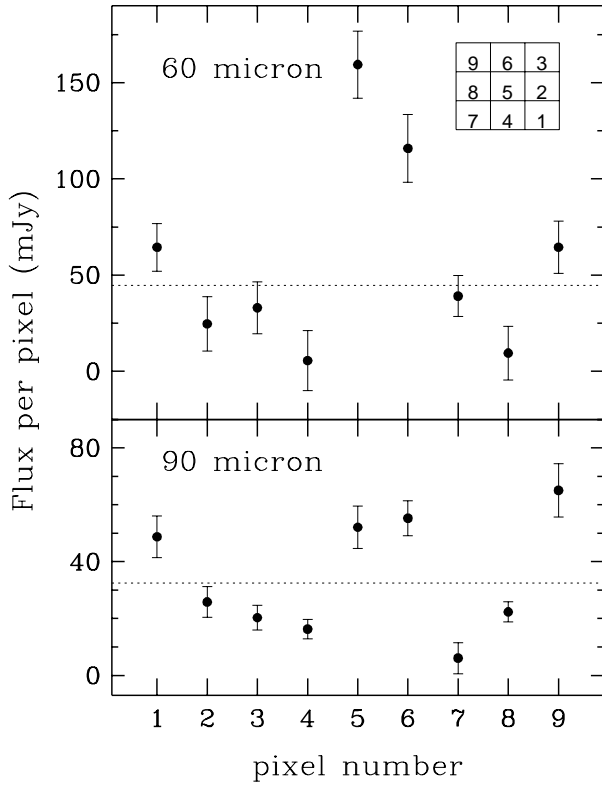


Fig. 1. The background subtracted flux per pixel. Upper panel: 60 μm , lower panel: 90 μm . The matrix in the upper panel depicts the relative pixel positions on the sky. The target was centered on pixel 5. The horizontal dotted lines are the zero levels obtained by taking the average of all pixels except for pixel 5.

Table 1. Summary of observations

| AOT | Filter | aperture | raster step |
|-------|--------|-----------|-------------|
| PHT03 | P_25 | 52'' | 90'' |
| PHT22 | C_60 | 46''x46'' | 180'' |
| | C_90 | 46''x46'' | 180'' |
| PHT22 | C_135 | 92''x92'' | 180'' |
| | C_180 | 92''x92'' | 180'' |

two identical calibration measurements of a grey body internal to ISOPHOT (the fine calibration source, FCS) were collected at the beginning and end of each raster scan. A summary of the observations is presented in Table 1.

Per raster step an exposure time of 128 sec was applied. For the C_60 and C_90 measurements we used the 3x3 C100 detector array. The target was therefore measured by the center pixel of the array during the integration on the second raster position. For the C_135 and C_180 measurements the 2x2 C200 detector array was used. Data reduction was performed with the ISOPHOT interactive analysis software package (PIA). The short measurements (32 sec) of the FCS were corrected for detector responsivity transients. For the longer integrations on the raster points (128 sec) this was not necessary. The target flux in each pixel was obtained by subtracting the average flux of the two background positions from the flux at the target position.

Table 2. Measured flux densities for ρ^1 Cnc

| Filter/Catalogue | λ [μm] | F_ν [mJy] | d F_ν [mJy] |
|------------------|-----------------------------|---------------|-----------------|
| P_25 | 24 | 170 | 20 |
| C_60 | 61 | 170 | 30 |
| C_90 | 95 | < 90 | - |
| C_135 | 161 | < 780 | - |
| C_180 | 185 | < 750 | - |
| IFSC | 12 | 981 | |
| IFSC | 25 | 241 | |
| IPSC | 60 | < 400 | |
| IPSC | 100 | < 1000 | |

The absolute calibration of the data utilized the pairs of FCS measurements related to each filter. At the time of writing this paper the accuracy in the absolute calibration of the FCS is better than 30% for P_25, C_60 and C_90. At the longer wavelengths the uncertainty is higher.

The background subtracted flux per pixel for the 60 and 90 μm measurements is presented in Fig. 1. For both wavelength bands all fluxes are larger than zero suggesting that the flux in the second pointing is systematically higher than the two background pointings. Since we expect the flux from the target predominantly in pixel 5 this observation indicates either that the background at the target position is higher or the presence of a non-linear long-term signal drift during the raster measurement. To correct for this we determined the mean flux among all pixels except pixel 5 and used this value as the new zero background level. Pixel 5 was excluded because it could contain emission from the star.

At 60 μm we find a significantly higher flux for pixel 5 and 6. At 90 μm the flux in these pixels is also higher, but is not significant. In both cases there are reasons to assume that the flux in pixel 6 is not reliable. It has been known for some time that (i) pixel 6 has a dark signal which is 4 to 6 times higher than the other pixels - a 10% variation in the dark signal would cause a flux variation of 70 mJy - and (ii) pixel 6 can show a signal drift which behaves differently compared to the other pixels. Since the background subtracted fluxes are very small compared to the total signal (5% for pixel 5), these anomalies in pixel 6 can show up in the difference signal. We therefore omit pixel 6 in further analysis.

Both the 135 and 180 μm observations exhibit background levels that are higher than the brightness level of the source position. We conclude that the star was not detected at these wavelengths. The uncertainty is dominated by the cirrus confusion noise.

The derived flux densities are given in Table 2, together with measurements and limits from IRAS. The uncertainties are the statistical errors obtained from the error propagation in the signals including FCS signals. The upper limit at 90 μm is 5 times the statistical error. The upper limits in the C_135 and C_180 bands are 5 times the estimated cirrus confusion noise on the target position obtained from the cartesian sum of the

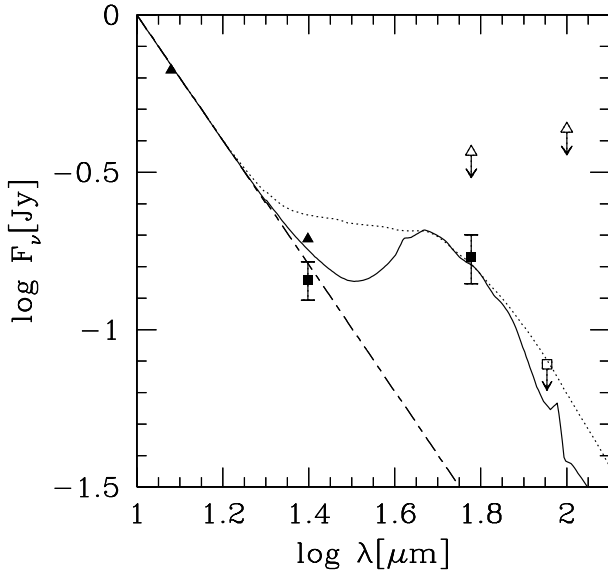


Fig. 2. The spectral energy distribution of ρ^1 Cnc. The dashed line is a Kurucz atmosphere fitted to the UBVJHKL and IRAS $12\ \mu\text{m}$ fluxes. The solid line indicates the flux of the disk model with icy grains described in the text. The dotted line shows a different model fit with ice-free dust grains. Triangular points are colour corrected measurements from the IRAS faint source catalogue. The limit shown at 60 and $100\ \mu\text{m}$ are taken from the IRAS point source catalogue. Squares are the new ISO measurements (also colour corrected). Open symbols with arrows indicate upper limits.

background subtracted flux of each pixel. Absolute calibration uncertainties are not included. The IRAS limits at 60 and $100\ \mu\text{m}$ are taken from the IRAS Point Source Catalogue (IPSC). The IRAS Faint Source Catalogue (IFSC) gives an upper limit of $105\ \text{mJy}$ at $60\ \mu\text{m}$, in conflict with our own measurement of $170\ \text{mJy}$. However, we believe the IFSC limit is not accurate in this case, probably corrupted by the influence of the nearby IR source IRAS 08494+2826. The $400\ \text{mJy}$ limit from the IPSC is consistent with our measurement.

The ISO measurements are plotted in Fig. 2 as squares. Also shown are the measurements from IRAS, plotted as triangles.

3. Discussion

3.1. Determination of the excess

In order to determine the infrared excess, we quantify the stellar component of the spectral energy distribution by fitting a Kurucz atmosphere model Kurucz1979 through the available visible, near-infrared and IRAS data of ρ^1 Cnc up to $12\ \mu\text{m}$. We used optical magnitudes from the Bright Star catalogue and infrared magnitudes from Gezari et al. (1993). A very satisfactory fit is obtained for the parameters $T_\star = 5250\text{K}$, $\log g = 4.0$, $z = 0$. Subtracting the infrared flux of this model from the observations, we derive no significant excess at $25\ \mu\text{m}$, an excess of $170 \pm 30\ \text{mJy}$ at $60\ \mu\text{m}$ and an upper limit of $90\ \text{mJy}$ for the excess at $90\ \mu\text{m}$.

3.2. Nature of the excess

We examine various possibilities that may cause such an excess. They have been discussed in detail by Aumann et al. (1984) and Backman & Paresce (1993) and we test them for ρ^1 Cnc.

1. The companion M5 star can be excluded as a source for the $60\ \mu\text{m}$ excess. At infrared wavelength the radiation from an M5 dwarf is typically less than 10% of the radiation of a G8 dwarf at the same distance. This is less than the error bars on our measurements and can be neglected. In addition, the companion is about $90\ \text{arcsec}$ away from ρ^1 Cnc. It is possible that it was visible in one of the two off-source positions of the $25\ \mu\text{m}$ measurement. However, in the critical $60\ \mu\text{m}$ measurement the position of the companion was always at the edge of the C100 array, thus not contaminating the detection in the central pixel 5.
2. The planet near ρ^1 Cnc can also be excluded. A planet with radius $1R_{\text{Jup}}$ would capture $\pi R_{\text{Jup}}^2 / 4\pi(0.11\text{AU})^2 \approx 4.7 \times 10^{-6}$ of the stellar radiation. This is one order of magnitude less than the 5×10^{-5} we see in the $60\ \mu\text{m}$ flux. Furthermore, the planet would re-radiate at a temperature near 1000K where it will be completely hidden in the stellar flux. At infrared wavelengths, the power of a 1000K Jupiter is typically only 10^{-3} of the stellar radiation.
3. Chance alignment with a cirrus knot. This cannot be ruled out completely, but alignment within $46\ \text{arcsec}$ (the pixel size of the C100 array) is unlikely.

Therefore we believe that the excess is due to the presence of a Vega-like disk.

3.3. A physical model for the disk

We now use the fluxes given in Sect. 3.1 to model a Vega-like disk. We calculate the emission from dust grains distributed in an optically thin disk around the star. We assume that the size distribution of the dust grains follows a power law $f(m) \propto m^{-1.83}$ as is commonly used for grains derived from collisional grinding. We use optical properties for cometary dust grains taken from Li & Greenberg (1997) with silicate core, organic refractory mantle, ice mantle (volume ratio 1:1:2), packed in fluffy aggregates with a porosity of 0.9. Grain masses in the model range from 10^{-11} and 10^{-8}g , corresponding to aggregate sizes between 2.2 and $22\ \mu\text{m}$. We distribute the grains in the disk with a surface density $\sigma \propto r^{-1.7}$, similar to what has been found for the β Pictoris disk Artymowicz et al. 1989. In order to reproduce the observed excess, we fit the total grain mass and the distance of the disk from the star.

Even though there is currently only an excess measured at $60\ \mu\text{m}$, the limits at 25 and $90\ \mu\text{m}$ help to constrain the model. The temperature of the dust grains surely cannot exceed 100K since this would produce an excess at $25\ \mu\text{m}$. Therefore, the grains have to be located outside $\approx 35\text{AU}$. On the other hand the temperature cannot be lower than 40K since this would require the $90\ \mu\text{m}$ flux to be as high as the $60\ \mu\text{m}$ flux. Also, the grains cannot be large compared to the $60\ \mu\text{m}$ wavelength of

the observation since this again would produce too much flux at $90\ \mu\text{m}$.

We can match the observations with a total dust mass of $1.2 \times 10^{-10} M_{\odot} = 4 \times 10^{-5} M_{\oplus}$, in a disk ranging from 50 to 60 AU from the star. The spectral energy distribution of this model is shown in Fig. 2. The fractional luminosity of the dust relative to the star is 5×10^{-5} . Disk mass and fractional luminosity are consistent with the results for other Vega-like disks. The mass estimate has to be seen as a lower limit since there could be larger bodies present but undetectable in the infrared.

Fig. 2 also shows for comparison the best fit with a similar dust grain model where the ice component has been left out (to the effect that the aggregate porosity increases to 0.95). The grains become warmer and have to be moved out to larger distances from the star (90 AU) in order to reach the same temperature as icy grains at 60 AU. Also we need more material ($4 \times 10^{-10} M_{\odot}$) to reproduce the $60\ \mu\text{m}$ flux. This model produces a less convincing fit, indicating that the ice model is more suitable to match the data.

3.4. Grain lifetimes

The radiation field of a G8 star is generally too weak to expel dust grains by radiation pressure. An upper limit for the lifetime of dust grains orbiting a star can always be given by the Poynting–Robertson time scale which is Burns et al. 1979, Backman and Paresce 1993

$$\tau_{\text{pr}} = 698 \rho a_{\mu} r_{\text{AU}}^2 Q_{\text{pr}}^{-1} L_{\star}^{-1} \text{ yr} \quad (1)$$

where a_{μ} is the grain radius in μm , Q_{pr} is the radiation pressure transfer efficiency of the grains, averaged over the stellar spectrum, ρ their specific density in g cm^{-3} , r_{AU} the distance from the star in AU and L_{\star} the luminosity of the star in solar units. At a distance of 60 AU and a grain size of $10\ \mu\text{m}$ ($\rho = 0.18\ \text{g cm}^{-3}$, $Q_{\text{pr}} \approx 0.4$, $L_{\star} \approx 0.6$) we find $\tau_{\text{pr}} = 18.8\ \text{Myr}$, much smaller than the age of the star (5 Gyr). Thus, also in ρ^1 Cnc the dust grains producing the excess need to be replenished in some way.

4. Conclusion

We have provided evidence that the planetary system of ρ^1 Cnc also hosts a Vega-like disk. The observations provide constraints to the disk structure which should comprise of not too large cometary dust particles at a distance of 50–60 AU, i.e. about 4 arcsec, from the star. The presence of ice seems to be required to match the observations. The Poynting–Robertson lifetime of the dust grains derived on the basis of the model shows that the dust grains in the disk must be replenished over the lifetime of the star, pointing to the existence of larger bodies, such as comets, from which the observed particles can be derived.

When the disks around main–sequence stars were first discovered, there was much speculation whether these disks were planetary systems in formation or, on the contrary, showed the failure of a system to produce planets. The age of some stars with excess made it obvious that this could not be due to on–going planet formation, but rather had to be a long–lasting phe-

nomenon. There have been observational indications that Vega-like disks and planets might co–exist. Some Vega-like disks show indications of inner “voids” Gillett 1986 with relatively lower dust densities. This has been attributed to the presence of planets Diner and Appleby 1986. HST images of the β Pic disk seem to indicate a small tilt of the inner disk which could be produced by a giant planet orbiting close to the inner edge of the disk in an inclined orbit Burrows et al. 1995. Our own solar system has both planets and a dust disk (the zodiacal dust) which, however, would be undetectable from nearby stars with instruments like ISO or IRAS. The same is true for dust presumably associated with the Kuiper Belt Backman et al. 1995.

The detection of a Vega-like excess associated with ρ^1 Cnc is the first evidence of both a planet and a disk around a star other than the Sun. We hope that this result will bring some clue to the discussion on formation and evolution of planetary systems.

Acknowledgements. The ISOPHOT data presented in this paper was reduced using PIA, which is a joint development by the ESA Astrophysics Division and the ISOPHOT consortium led by the Max Planck Institute for Astronomy (MPIA), Heidelberg. Do Kester provided valuable help in examining various IRAS data of ρ^1 Cnc. This research has made use of the SIMBAD database, operated at CDS, Strasbourg, France. CD acknowledges support from the Stichting Astronomisch Onderzoek (ASTRON, project nr. 781-76-015).

References

- Artymowicz, P., Burrows, C., and Paresce, F.: 1989, *APJ* 337, 494
- Aumann, H. H.: 1985, *PASP* 97, 885
- Aumann, H. H., Gillett, F. C., Beichmann, C. A., deJong, T., Houck, J., Low, F. J., Neugebauer, G., Walker, R., and Wesselius, P. R.: 1984, *APJ* 278, 23
- Backman, D. E., Dasgupta, A., and Stencel, R. E.: 1995, *APJ* 450, L35
- Backman, D. E. and Paresce, F.: 1993, in E. H. Levy and J. I. Lunine (eds.), *Protostars and Planets III*, University of Arizona Press, Tucson
- Baliunas, S. L., Henry, G. W., Donahue, R. A., Fekel, F. C., and Soon, W. H.: 1997, *APJ* 474, L229
- Burns, J. A., Lamy, P. L., and Soter, S.: 1979, *Icarus* 40, 1
- Burrows, C. J., Krist, J. E., Stapelfeldt, K. R., and Team, W. I. D.: 1995, *Bull. American Astron. Soc.* 187, 3205+
- Butler, R. P., Marcy, G. W., Williams, E., Hauser, H., and Shirts, P.: 1997, *APJ* 474, L115
- Diner, D. J. and Appleby, J. F.: 1986, *Nature* 322, 436
- Gezari, D. Y., Schmitz, M., Pitts, P. S., and Mead, J. M.: 1993, *Catalogue of Infrared Observations*, NASA RP-1294
- Gillett, F. C.: 1986, in F. P. Israel (ed.), *Light on Dark Matter*, pp 61–69, Reidel, Dordrecht
- Kessler, M., Steinz, J., and et al., M. A.: 1996, *A&A* 315, L27
- Kurucz, R. L.: 1979, *APJs* 40, 1
- Lemke, D., Klaas, U., and et al., J. A.: 1996, *A&A*
- Li, A. and Greenberg, J. M.: 1997, *A&A* 323, 566
- Mayor, M. and Queloz, D.: 1995, *Nature* 378, 355